Received: 12 December 2018 | Revised: 20 May 2019 | Accepted: 27 June 2019

DOI: 10.1002/aic.16714

SOFT MATTER: SYNTHESIS, PROCESSING AND PRODUCTS

AIChE JOURNAL

High-gravity-assisted synthesis of aqueous nanodispersions of organic fluorescent dyes for counterfeit labeling

Xiong Yin[1,2,3] | Qian Sun[1,2,3] | Dan Wang[1,2,3] | Alexander F. Routh[4] | Yuan Le[1,3] | Jie-Xin Wang[1,2,3] | Jian-Feng Chen[1,2,3]

[1]State Key Laboratory of Organic-Inorganic Composites, Beijing University of Chemical Technology, Chaoyang, Beijing, China

[2]Beijing Advanced Innovation Center for Soft Matter Science and Engineering, Beijing University of Chemical Technology, Chaoyang, Beijing, China

[3]Research Center of the Ministry of Education for High Gravity Engineering and Technology, Beijing University of Chemical Technology, Chaoyang, Beijing, China

[4]Department of Chemical Engineering and Biotechnology, University of Cambridge, Cambridge, UK

Correspondence
Jie-Xin Wang, State Key Laboratory of Organic-Inorganic Composites, Beijing University of Chemical Technology, Chaoyang, Beijing 100029, China.
Email: wangjx@mail.buct.edu.cn

Funding information
National Key Basic Research Program of China, Grant/Award Number: 2015CB932100; National Key Research and Development Program of China, Grant/Award Number: 2016YFA0201701/2016YFA0201700; National Natural Science Foundation of China, Grant/Award Number: 21622601, 21878015 and 21576022

Abstract

Organic fluorescent dyes have attracted wide interest because of their high photoluminescence quantum efficiencies. However, there are several application limitations arising from their hydrophobicity, poor dispersity and large particle sizes. These problems can be improved by preparing nanoparticles with a small size. Herein, we present a continuous approach to efficiently prepare an aqueous nanodispersion of water-insoluble organic fluorescent dye Nile red (NR) with monodispersed and uniform nanoparticles (35 nm) by high-gravity antisolvent precipitation in a rotating packed bed (RPB). In contrast, NR nanodispersions prepared using a traditional batch stirred tank (ST) had a broad size distribution (20–150 nm). Due to its small size effect and good dispersity in water, the RPB nanodispersion displayed significantly increased saturation solubility and much stronger fluorescent intensity compared to raw NR, and was obviously superior to the ST counterpart. Furthermore, NR nanodispersions were mixed with ink to draw fluorescent patterns on paper for counterfeit labeling.

KEYWORDS
aqueous nanodispersion, counterfeit labeling, high-gravity antisolvent technique, monodispersed Nile red nanoparticles

1 | INTRODUCTION

Fluorescence techniques have played an important role in many fields, such as biomedical imaging,[1,2] counterfeit labeling,[3] biochemical sensing[4] and optoelectronic materials.[5] The commonly used fluorescent labeling agents include traditional classes of organic fluorescent dyes,[6,7] fluorescein[8] and lanthanide chelates,[9] as well as new fluorescent labels based on nanoparticles, such as semiconductor quantum dots (QDs),[10,11] rare-earth-doped upconversion nanoparticles,[12,13] carbon dots,[14-16] and dye-doped polymeric nanoparticles.[17] Among these fluorescent labeling agents, the organic fluorescent dyes have been developed and used because of their remarkably high photoluminescence quantum efficiencies.[6,18,19] However, most organic fluorescent dyes have limitations such as hydrophobicity, poor dispersity, large particle sizes, and wide size distributions,[20] which present a significant challenge for biological applications. At present, in order to overcome these problems, organic fluorescent dyes are prepared into nanomaterials. It is an important development direction to improve the properties of organic fluorescent dyes through the formation of nanostructures. Specifically, it is advantageous to make conventional organic fluorescent dyes into nanoparticles with high water solubility, good dispersity, and small and uniform particle sizes.

Various methods have been reported for the preparation of organic fluorescent dye nanoparticles, including ball milling,[21] ion association,[22] self-assembly method,[23,24] micro-emulsion method,[25,26] laser fabrication,[27] vapor deposition,[28] supercritical fluid technology,[29] and antisolvent precipitation.[30,31] Among these techniques, antisolvent precipitation has a great prospect, because of its low cost, convenient processing, and easy industries scale-up.[32] During precipitation, the formation of uniform nanoparticles mainly depends on the control of supersaturation level through the mixing process. The instantaneous and homogeneous mixing of solvent and antisolvent is crucial to the achievement of a nano-scale and narrow particle size distribution. However, the complete control of a homogeneous mixing process is difficult in a commonly used batch stirring tank (ST), particularly when large volumes of solution are involved. Thus, various techniques for process intensification are being developed to obtain a high mixing efficiency for the preparation of nanoparticles with a narrow particle size distribution.

A rotating packed bed (RPB) as process intensification device can generate a high-gravity environment of tens to hundreds of gravitational acceleration (g). In a typical RPB, liquids pass through the porous packing of the equipment and are spread or split into micro/nano droplets, threads, and thin films by the powerful shear, thereby leading to a high intensification of micromixing and mass transfer between the fluid elements.[33-35] During nanoparticle preparation, the RPB allows the reaction or precipitation process to proceed at a uniform concentration, temperature and supersaturation, which is beneficial to the homogeneous nucleation and growth of particles. In recent years, RPB has been successfully applied in the preparation of various organic and inorganic nanoparticles, providing a promising industrial platform for the production of nanomaterials.[36-38] Until now, there are very few related reports on the preparation of aqueous nanodispersions of water-insoluble organic fluorescent dye using the RPB.

In this article, we report an efficient and continuous approach to prepare a transparent aqueous nanodispersion of Nile red (NR, a representative organic fluorescent hydrophobic dye) with monodispersed and uniform nanoparticles by antisolvent precipitation in a high-gravity RPB for the first time. In the study, the effects of process parameters including surfactant addition, solvent/antisolvent (S/AS) ratio and temperature on the particle size and dispersity were explored. The optimum conditions were achieved. Compared to raw NR, the resultant NR nanodispersions displayed significantly increased saturation solubility and much stronger fluorescent intensity in aqueous solution. It was also superior to its counterpart prepared in a batch ST. Furthermore, NR nanodispersions were mixed with commercial ink to draw a pattern on paper, maintaining their fluorescence in the solid state. This is promising for a potential use in counterfeit labeling, solid-state fluorescent sensing and fluorescent composites with a high-performance.

2 | EXPERIMENTAL

2.1 | Materials and equipment

Nile red (NR, 98%) was bought from Shanghai Yuanye Biochemical Technology Co., Ltd. Polysorbate 80 (Tween 80) was purchased from Sinopharm Chemical Reagent Beijing Co., Ltd. Poly(vinylpyrrolidone) (PVP K30) and sodium dodecyl sulfate (SDS) were provided by Tianjin Heowns Biochemical Technology Co., Ltd. Analytical reagent grade acetone was purchased from Beijing Chemical Works. Deionized water obtained from a Hitech-K flow water purification system (Shanghai Hogan Scientific Instrument Co. Ltd., China) was used for all experiments.

The experimental setup for the preparation of an aqueous NR nanodispersion with monodispersed and uniform nanoparticles is schematically displayed in Figure 1. The key component of the whole procedure is the RPB, including a stainless wire-mesh packed rotator, a fixed casing, two liquid inlets, and a suspension outlet. The rotator is installed inside the fixed casing and rotated at an adjustable speed. More details about the structure of the RPB can be found in our previous work.[33,37,39]

2.2 | Preparation of aqueous NR nanodispersions with monodispersed and uniform nanoparticles

In a typical high-gravity antisolvent precipitation process, acetone and deionized water were used as solvent and antisolvent, respectively. Firstly, raw NR was dissolved in 30 mL of acetone at 25°C to form a solution with a concentration of 10 μg·mL^{-1} and placed in container 1. A 0.8 mg·mL^{-1} Tween 80 aqueous solution of 210 mL was stored in container 2. Afterwards, the flow rates of the solvent and the antisolvent were set to 85 and 600 mL·min^{-1}, respectively. The streams from the containers were simultaneously pumped through the flow meters into the RPB with a rotation speed of 500 rpm. Both fluids were sprayed onto the inner edge of the rotator and mixed in the packed bed zone to produce nanoparticles. After that, the collected suspension was evaporated at 40°C in a rotary vacuum evaporator to remove the acetone. Finally, an optically clear aqueous NR nanodispersion with monodispersed and uniform nanoparticles was achieved.

As a control experiment, the suspension was also similarly prepared in a stirred tank. Briefly, 30 mL of 10 μg·mL^{-1} NR solution in

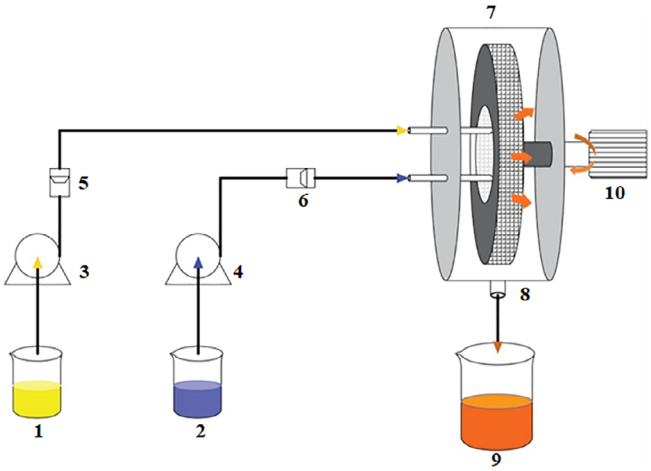

FIGURE 1 Schematic diagram of experimental setup for high-gravity antisolvent precipitation process (legend: (1) solvent container; (2) antisolvent container; (3, 4) pumps; (5, 6) flow meters; (7) RPB; (8) liquid outlet; (9) outlet container; and (10) motor) [Color figure can be viewed at wileyonlinelibrary.com]

acetone was rapidly added into 210 mL of 0.8 mg·mL^{-1} Tween 80 aqueous solution to prepare a mixed suspension with vigorous stirring. After stirring for 30 s, the suspension then evaporated to obtain the final NR nanodispersion.

2.3 | Saturation solubility studies

NR saturation solubility was measured for NR nanodispersions and raw NR with the same composition. The samples were stirred constantly for 48 h in a thermostated water bath at 37°C, and were then withdrawn and centrifuged at 12,000 rpm for 60 min. The supernatant was further centrifuged at 12,000 rpm for 30 min. Finally, the clear filtrate was analyzed with a UV spectrophotometer at 550 nm to obtain the NR concentration. The measurement was repeated three times.

2.4 | Characterization

The size, morphology and dispersity of NR nanoparticles were imaged by a transmission electron microscopy (TEM) (Hitachi HT7700, Japan) at an accelerating voltage of 100 kV. The particle size distributions of NR nanoparticles were obtained by measuring TEM images with image analysis and processing software (Image-Pro Plus 6.5, Media Cybernetics Inc., USA). The geometric standard deviations (σ_g) of NR nanoparticles were obtained by a data analysis software (Origin 9, OriginLab Corp., USA). If σ_g is close to 1, lognormal distribution is approximately equal to normal distribution. Dynamic light scattering (DLS) data of NR nanoparticles were obtained using a Malvern Zetasizer Nano ZS90 instrument. Fourier transform infrared (FTIR) spectroscopy data were recorded in the wavenumber range of 4,000–400 cm^{-1} with a Nicolet 6700 spectrometer (Nicolet Instrument Co., USA). The resulting NR nanodispersion was characterized using a UV–Vis spectrometer (UV-2501, Shimadzu, Japan) in the range of 200–800 nm. The photoluminescence (PL) spectra were obtained using a fluorescence spectrophotometer (Edinburgh Instruments FS5 fluorescence spectrometer, UK). Fluorescence quantum yields of the NR nanodispersion and the NR acetone solution with a low concentration of 0.03 μg·mL^{-1} (UV absorbance was 0.08) were determined by a fluorescence spectrometer (Edinburgh Instruments FLS980 spectrometer, UK).

3 | RESULTS AND DISCUSSION

During antisolvent precipitation, surfactants can be used to control the growth and agglomeration of nanoparticles by electrostatic and steric stabilization. In order to investigate the effect of surfactant on the particle size and distribution of the formed nanoparticles, three kinds of surfactants were used, including Tween 80 (a biodegradable and common nonionic surfactant), PVP K30 (a common nonionic polymer surfactant), and SDS (an anionic surfactant). The concentration of the three surfactants used to prepare the particles was all 1 mg/mL. Figure 2 shows the TEM images and corresponding digital photographs of NR dispersions prepared by high-gravity antisolvent precipitation using different surfactants. It can be seen that the prepared NR particles aggregated and precipitated in the absence of surfactant, indicating that the surfactant was required for this system (Figure 2a). However, the size and the dispersity of NR nanoparticles were not obviously improved when PVP K30 and SDS were added. As shown in Figure 2b,c, the dispersions rapidly precipitated and were almost colorless. The addition of Tween 80 may help to form a transparent and pink aqueous dispersion of nearly monodispersed NR nanoparticles with an average particle size of 65 nm (Figure 2d). In the presence of Tween 80, agglomeration did not occur. This is possibly because the nonpolar tails of Tween 80 molecules adsorb onto the exposed strong hydrophobic surfaces of

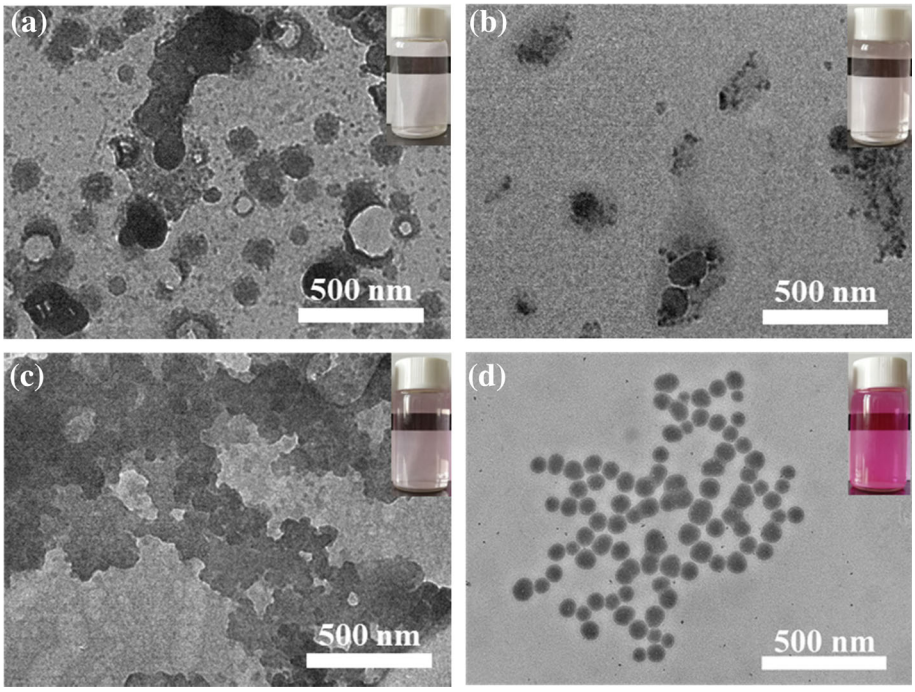

FIGURE 2 TEM images of NR particles prepared with (a) no surfactant (b) PVP, (c) SDS, and (d) Tween 80. The insets are digital photographs of corresponding NR dispersions. TEM, transmission electron microscopy; NR, Nile red; PVP, poly(vinylpyrrolidone); SDS, sodium dodecyl sulfate [Color figure can be viewed at wileyonlinelibrary.com]

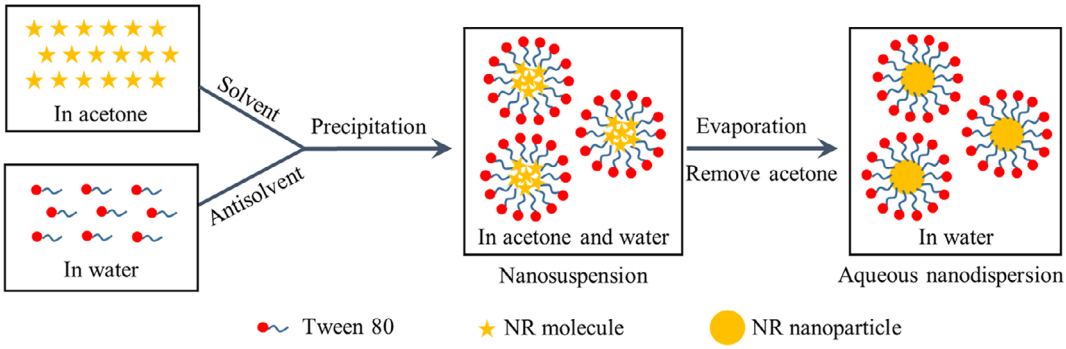

SCHEME 1 The major steps of the preparation of aqueous NR nanodispersions. NR, Nile red [Color figure can be viewed at wileyonlinelibrary.com]

NR nanoparticles, and form a sterically stabilizing layer around the nanoparticles preventing the particles from agglomerating (Scheme 1).[40] Other surfactants may not effectively adsorb on the surface of the formed NR nanoparticles, resulting in a rapid agglomeration of the primary particles. Therefore, Tween 80 was chosen as the surfactant in our subsequent experiments. In addition, the zeta potential values of NR nanodispersions remained essentially unchanged with the increase of Tween 80 concentration (Figure S1). This indicates that electrostatic stabilization has little effect, and steric stabilization plays a major role on this process.

Figure 3 presents the effect of Tween 80 concentration on the size and dispersity of NR nanoparticles. The corresponding particle size distributions of NR nanoparticles prepared at different Tween 80 concentrations are shown in Figure S2. When the Tween 80 concentration was increased from 0.2 to 1.0 mg/mL, the average size of NR nanoparticles decreased from 110 to 64 nm (σ_g were 1.16, 1.12, 1.11, 1.12, and 1.15 in order) and then plateaued. The nanoparticles exhibited a narrower size distribution, a more spherical shape and better dispersity, indicating that the degree of particle agglomeration was weakened. In addition, the red color of NR nanodispersions gradually became deeper with an increasing amount of surfactant, suggesting that the dispersity of the nanodispersion was improved. A stable and transparent NR aqueous nanodispersion can be obtained when the concentration of Tween 80 was 0.8 mg/mL or more. As the surfactant concentration increased, the particle size reduced. A possible reason is that more surfactant molecules reduce the interfacial tension at the solid–liquid interface, resulting in a higher rate of nucleation and the subsequent formation of smaller particles. Another possible mechanism is that the adsorption of the surfactant molecules onto the surface of the nuclei during the nucleation process allows by steric repulsion the nanoparticles to avoid growth.[32,41]

In addition to the surfactant, the antisolvent/solvent (AS/S) ratio is also an important factor for the precipitation, since the driving force in this process is the supersaturation of a solution, induced by the rapid mixing of solvent and antisolvent. To investigate the effect of AS/S ratio, the flow rate of antisolvent was fixed at 600 mL/min, whilst the flow rate of NR solution was adjusted to obtain various AS/S ratios. Figure 4 shows the TEM images, corresponding average particle sizes and digital photographs of NR nanodispersions at different AS/S ratios. The corresponding particle size distributions of NR nanoparticles prepared at different AS/S ratios are shown in Figure S3. It could be seen that the as-prepared NR nanoparticles had a notably decreased particle size from 85 to 35 nm (σ_g were 1.15, 1.13, 1.11, and 1.14 in order), narrower size distribution and better dispersity when increasing AS/S ratio from 1 to 7. Furthermore, the inset of Figure 4f showed that the red color of NR nanodispersions gradually deepened owing to the smaller size and better dispersity of nanoparticles. This can be explained as follows. Precipitation mainly includes two steps: nucleation and particle growth. The nucleation rate is given by Equation (1)[42]:

$$\frac{dN}{dt} \propto \exp\left(-\frac{16\pi\sigma^3 V_S^2}{3k^3T^3(\ln S)^2}\right) \quad (1)$$

where σ is the interfacial tension, V_s is the volume of the solute molecule, k is the Boltzmann constant, T is the temperature, and S is the supersaturation defined as the ratio of NR concentration over the saturation solubility in the mixed solvent. The rate of nucleation is largely dependent on the degree of supersaturation, and this heavily affects the final particle size. By increasing the AS/S ratio, the supersaturation was increased by the reduction in saturation concentration, resulting in a faster nucleation rate and smaller critical nucleus size. The particle growth rate can be expressed as[43]

$$\frac{dr}{dt} = K_g\left(C_i - \boldsymbol{C}^*\right)^b \quad (2)$$

where r is the particle radius, K_g is the rate constant of particle growth, and C_i is the solute concentration on the surface of particles and C^* is the saturation concentration. The value of the parameter b is generally between 1 and 3, and it is found to increase monotonically with temperature. The increased AS/S ratio reduced the solute concentration on the surface of the formed NR particles. Therefore, a decrease in the value of $C_i - C^*$ led to a slower particle growth rate, thereby resulting in a smaller particle size. However, further increasing AS/S ratio to 10 caused an obvious increase of average particle size again and a partial agglomeration of nanoparticles. This result is because the flow rate of the NR solution is too small to sufficiently premix at a higher AS/S ratio, thereby generating an uneven supersaturation degree and inadequate micromixing. Thus, the larger particles and the agglomeration were easily formed.

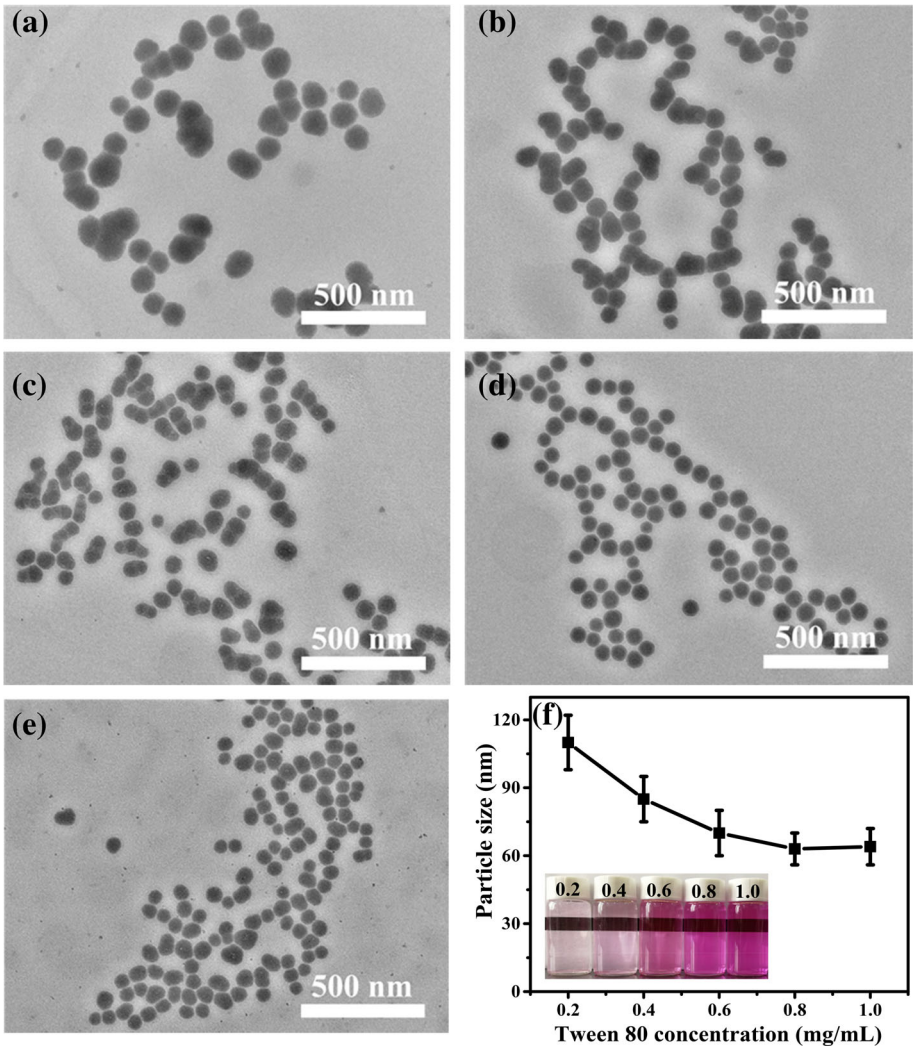

FIGURE 3 TEM images of NR nanoparticles prepared at different Tween 80 concentrations: (a) 0.2 mg/mL, (b) 0.4 mg/mL, (c) 0.6 mg/mL, (d) 0.8 mg/mL, and (e) 1 mg/mL. (f) The average sizes of nanoparticles prepared at different Tween 80 concentrations. The insets are digital photographs of corresponding NR dispersions. NR, Nile red; TEM, transmission electron microscopy [Color figure can be viewed at wileyonlinelibrary.com]

Figure 5 shows the TEM images of NR nanoparticles prepared at different temperatures and the corresponding particle size distributions. When the temperature was raised from 25 to 45°C, the average particle size increased from 39 to 77 nm (σ_g were 1.14 and 1.16, respectively), and particles gathered together. Such results can be explained by the following reasons. Firstly, a lower temperature caused a higher supersaturation level, which led to a smaller critical nucleus size. In addition, this reduced the rate of diffusion, and consequently the particle growth rate. In consideration of the effect of temperature on parameter b in Equation (2), smaller particles can be prepared at lower temperatures. However, when the temperature was as low as 10°C, the average particle diameter increased to 48 nm (σ_g was 1.15), and the particles were slightly aggregated. Furthermore, it can be seen from Figure 5a that part of the nanoparticles were obtained with hollow structures. This is possibly because Tween 80 molecules have a reduced affinity with NR nanoparticles at a low temperature, and do not adsorb well on the surface of NR particles.[44] In this case, the stabilization of nanoparticles by Tween 80 becomes less effective, and Tween 80 may not control the growth of particles and prevent agglomeration. Therefore, room temperature (25°C) can satisfy the requirement of preparing uniform NR nanoparticles under high-gravity environment.

To better understand the big differences of three surfactants in the preparation process, the similar systematic investigations for other surfactants (PVP and SDS) have also been conducted, such as surfactant concentration, solvent/antisolvent ratio and temperature, but have not achieved the desired results. The NR nanoparticles with good dispersion cannot be obtained by changing these process parameters, which could be observed in the corresponding TEM images of Figure S4–S6.

Figure 6 presents the TEM images, particle size distributions, FTIR spectra and saturation solubility of raw NR and NR nanodispersions prepared by RPB and ST under optimum conditions and the corresponding digital photographs. The raw NR exhibited an irregular shape with the particle size ranging from several micrometers to tens of micrometers, and could not be dispersed in water (Figure 6a). NR nanodispersion prepared by RPB showed a regular spherical morphology with an average size of 35 nm (σ_g was 1.14). By contrast, the counterpart prepared by ST had an irregular particle morphology with an average size of 82 nm (σ_g was 1.61) and a broad size distribution ranging from 20 to 150 nm (Figure 6b–e). The size distributions of NR

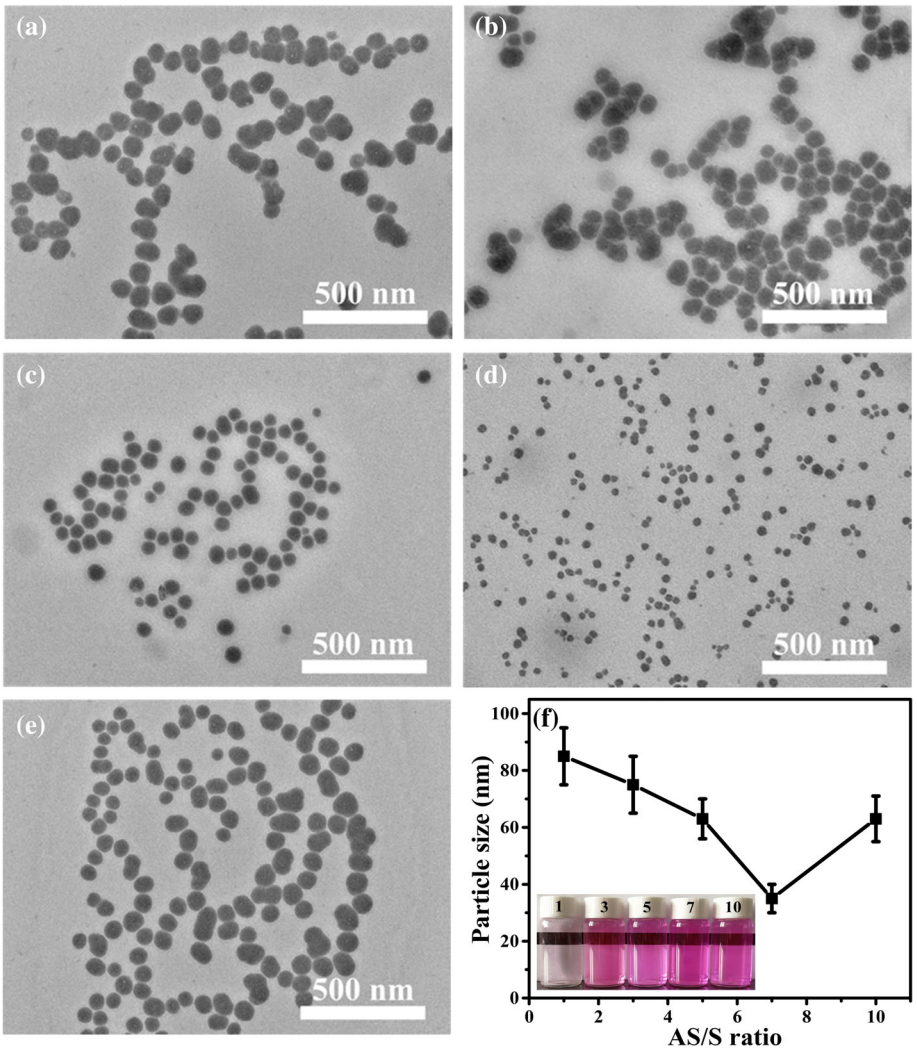

FIGURE 4 TEM images of NR nanoparticles prepared at different AS/S ratios: (a) AS/S = 1, (b) AS/S = 3, (c) AS/S = 5, (d) AS/S = 7, and (e) AS/S = 10. (f) The average sizes of nanoparticles prepared at different AS/S ratios. The insets are digital photographs of corresponding NR dispersions. AS/S, antisolvent/solvent; NR, Nile red; TEM, transmission electron microscopy [Color figure can be viewed at wileyonlinelibrary.com]

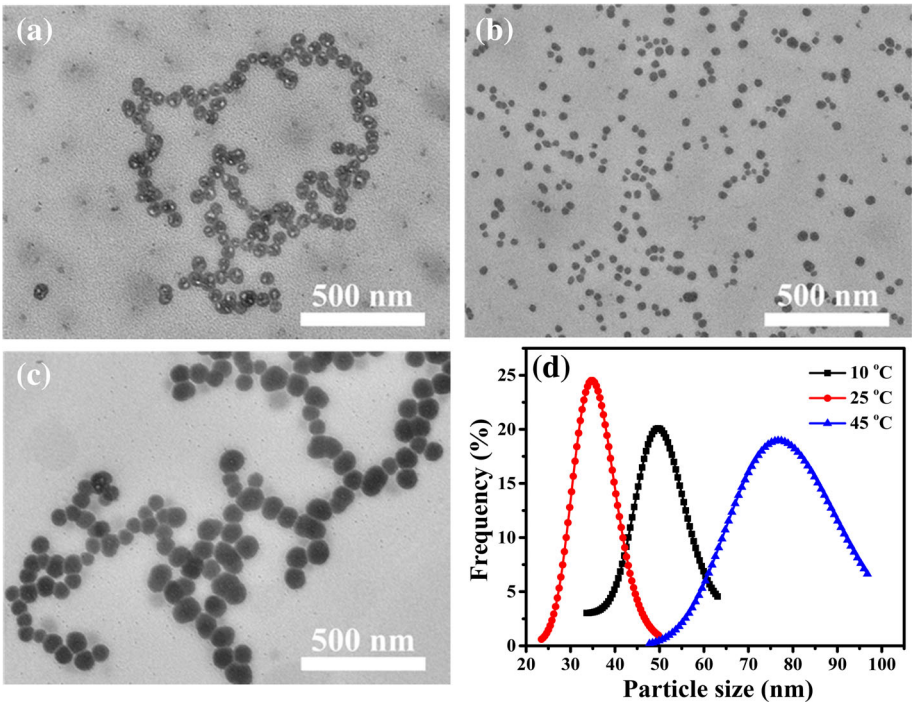

FIGURE 5 TEM images of NR nanoparticles prepared at different temperatures: (a) 10°C, (b) 25°C, and (c) 45°C. (d) Particle size distributions of NR nanoparticles prepared at different temperatures. NR, Nile red; TEM, transmission electron microscopy [Color figure can be viewed at wileyonlinelibrary.com]

nanoparticles were also measured by DLS, as shown in Figure S7. The results showed that the average size of NR nanoparticles prepared by RPB was about 70 nm, and the particle size distribution was relatively narrow (20–300 nm), while the average size of nanoparticles prepared by ST was about 105 nm and the particle size distribution was much broader (20–5 μm). The above results demonstrated that RPB owned the unique advantage of greatly intensifying the micromixing during the antisolvent precipitation process, thereby ensuring a highly homogeneous mixing environment. To obtain nanoparticles and control the particle size distribution during preparation, the homogenous concentration and supersaturation should be created and maintained before particle nucleation. Consequently, the nanoparticles, which were produced using RPB, were more uniform and smaller than those prepared in a conventional ST. Under optimum process conditions, the production capacity of NR nanoparticles in a laboratory-scale rotating packed bed (RPB) with a continuous operation can be achieved to 50 mg/h. The high-gravity antisolvent precipitation method in this study can provide a universal and convenient platform for large-scale production of fluorescent nanoparticles. The FTIR spectra of NR nanodispersions prepared using RPB and ST showed similar characteristic bands (Figure 6f). Compared

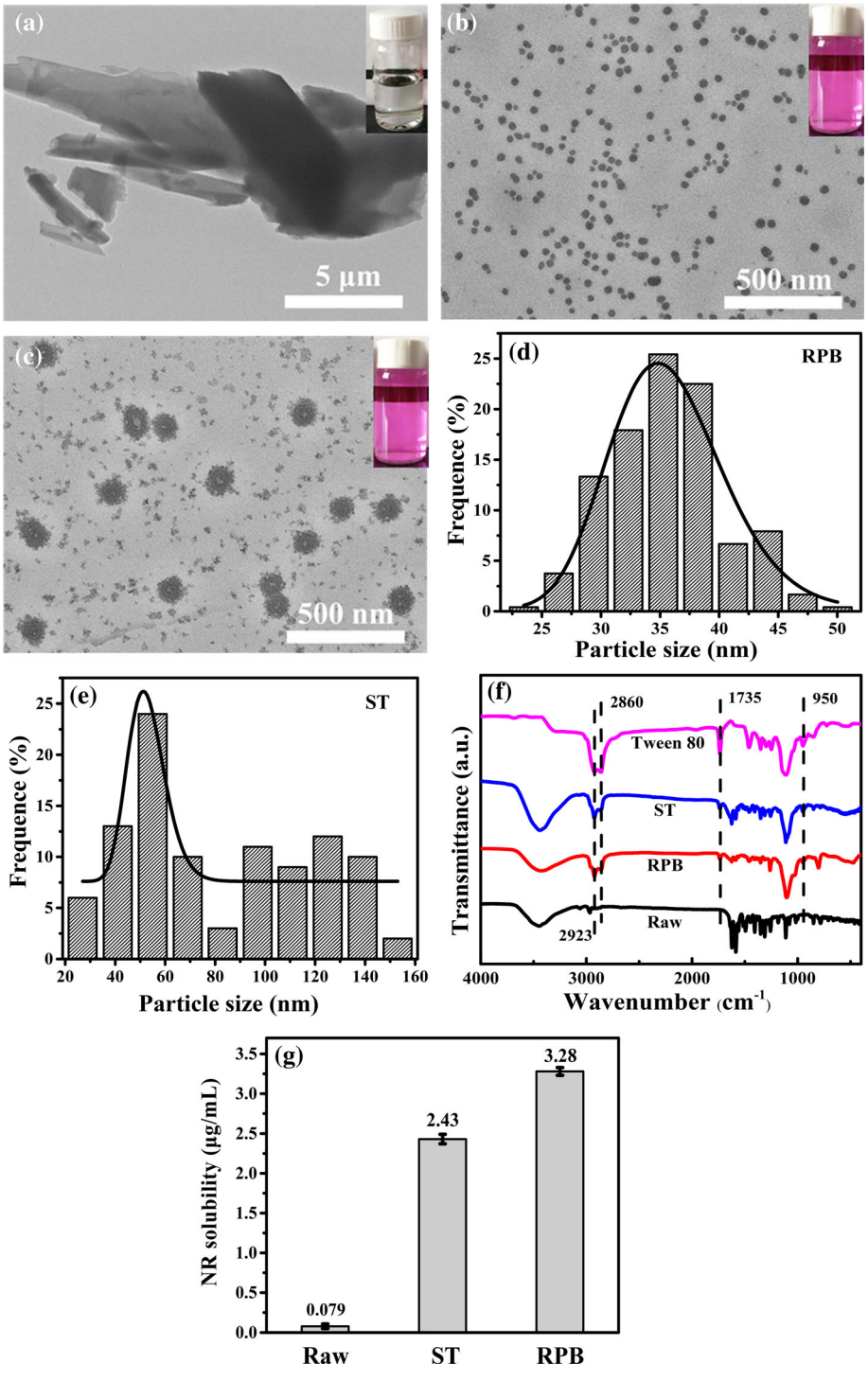

FIGURE 6 (a, b, c) TEM images, (d, e) particle size distributions of NR nanoparticles prepared by RPB and ST, (f) FTIR spectra, and (g) saturation solubilities of raw NR, nanoparticles from RPB and ST. FTIR, Fourier transform infrared; NR, Nile red; RPB, rotating packed bed; ST, stirred tank; TEM, transmission electron microscopy [Color figure can be viewed at wileyonlinelibrary.com]

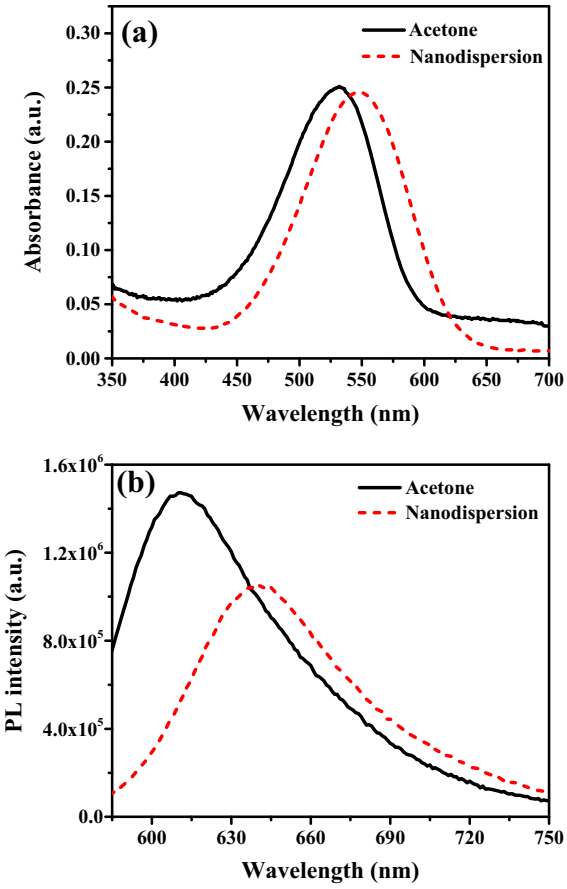

FIGURE 7 (a) UV-vis absorption spectra and (b) PL spectra of NR in acetone and NR nanoparticles in aqueous nanodispersions. NR, Nile red; PL, photoluminescence [Color figure can be viewed at wileyonlinelibrary.com]

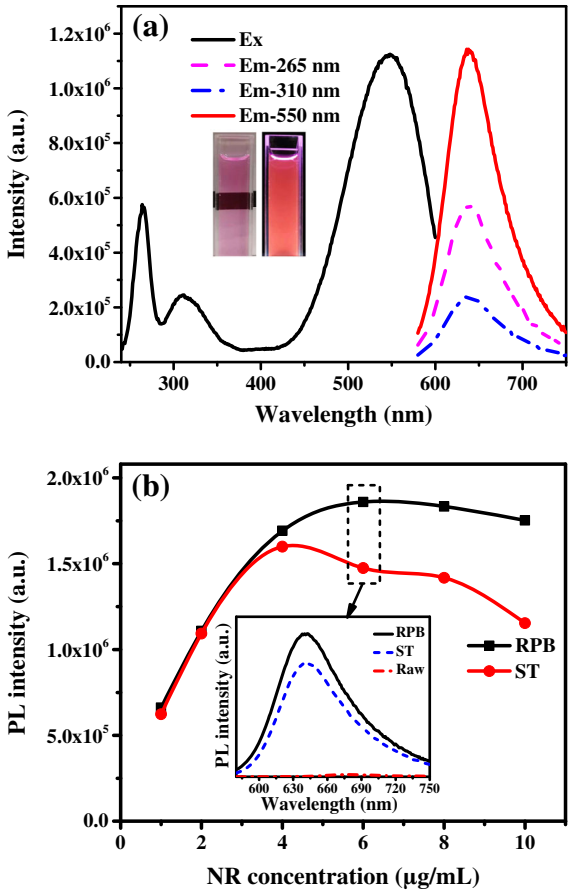

FIGURE 8 Fluorescent properties of NR nanodispersion. (a) PL excitation and emission spectra of NR nanodispersion prepared by RPB. (b) Comparison of PL intensity (640 nm) of NR nanodispersions with different NR concentrations prepared by RPB and ST (λ_{ex} = 550 nm). NR, Nile red; PL, photoluminescence; RPB, rotating packed bed [Color figure can be viewed at wileyonlinelibrary.com]

with raw NR and Tween 80, both NR nanodispersions exhibited four characteristic peaks of Tween 80. The strong peaks at 2923 and 2,860 cm^{-1} were assigned to asymmetric and symmetric stretching of methylene groups (—CH_2—). The peaks at 1735 and 950 cm^{-1} were referred to the C═O (ester group) stretching vibrations and the bending vibrations of C—H.[45] This indicated that NR nanoparticles were successfully modified by using Tween 80 as a surfactant. In addition, the saturation solubilities of both nanodispersions prepared using RPB and ST were also measured for comparison with raw NR in water at 37°C. The saturation solubility of NR nanoparticles prepared using RPB was 3.28 μg·mL^{-1}, which was approximately 41 times higher than those of raw NR, and was 1.35 times of NR nanoparticles prepared by ST (Figure 6g). The huge saturation solubility difference of raw NR and NR nanoparticles is not only attributed to the solubilizing and wetting function of Tween 80, but also to the reduction in particle size, according to the Freundlich–Ostwald Equation (3)[21,46]:

$$\log \frac{C_S}{C_\infty} = \frac{2\sigma V}{2.303RT\rho r} \quad (3)$$

where C_S is the saturation solubility, C_∞ is the solubility of the solid consisting of large particles, σ is the interfacial tension substance, V is the molar volume of the particle material, R is the gas constant, T is the absolute temperature, ρ is the density of the solid, and r is the particle radius. However, the difference of the two products between RPB and ST is mainly because of the smaller size and better dispersity of the former.

The NR acetone solution and aqueous dispersion of NR nanoparticles were characterized using a UV-vis spectrophotometer and a fluorescence spectrophotometer, respectively. Figure 7 shows the UV-vis absorption spectra and PL spectra of NR in acetone, and NR nanoparticles in aqueous nanodispersions. As shown in Figure 7, the maximum absorption wavelength of NR nanoparticles in aqueous nanodispersions was 550 nm, while the maximum absorption wavelength of NR in acetone was 530 nm, indicating that the absorption peak wavelength shifted 20 nm. However, compared with the NR acetone solution, the fluorescence peak wavelength of the aqueous nanodispersion was shifted from 610 to 640 nm. In addition, the fluorescence quantum yield of the NR nanodispersion was 67.54%, and the fluorescence quantum yield of the NR acetone solution was 93.28%. The differences are possibly because that the NR nanoparticles are "dispersed" in water and the NR molecules are "dissolved" in acetone.[18] After NR acetone solution and aqueous

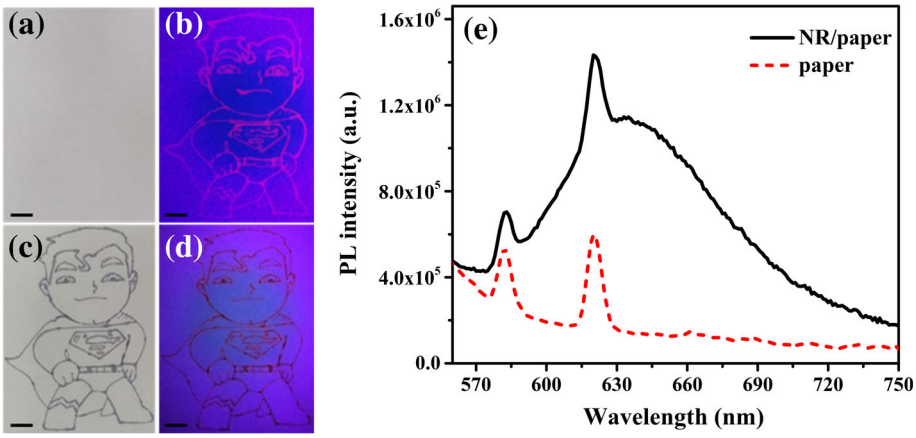

FIGURE 9 Photographs of NR patterns drawn using NR nanodispersion under (a) daylight and (b) 254 nm UV lamp excitation, and using NR ink under (c) daylight and (d) 254 nm UV lamp excitation. The scale bar is 1 cm. (e) PL spectra of the NR nanoparticles in the solid state and background fluorescence of the paper (λ_{ex} = 254 nm). NR, Nile red; PL, photoluminescence [Color figure can be viewed at wileyonlinelibrary.com]

dispersion of NR nanoparticles were continuously irradiated for 2 hr on a 254 nm UV lamp, their fluorescence spectra remained substantially unchanged, indicating that NR acetone solution and aqueous dispersion of NR nanoparticles had relatively high photostabilities (Figure S8).

Figure 8 shows the photoluminescence (PL) spectra of NR nanodispersion prepared using RPB and a comparison of the fluorescence intensity (640 nm) of NR nanodispersions with different NR concentrations prepared by RPB and ST. As shown in Figure 8a, the NR nanodispersions had three peaks at the excitation spectrum, which should be excited to generate strong fluorescence at the emission wavelength of 640 nm. The maximum excitation wavelength in the ultraviolet wavelength range was 265 nm, while that in the visible light wavelength range was 550 nm. The NR nanodispersion can emit fluorescence after these two different light excitations, and is beneficial for its multifunctional applications, such as bioimaging, counterfeit labeling, and fluorescent film materials.[47] As can be seen from the digital images in the insets of Figure 8a, transparent NR nanodispersions exhibited bright red emission under UV excitation (254 nm). Meanwhile, aqueous NR nanodispersion prepared using this method can emit strong fluorescence without using an organic solvent, and have the advantages of non-toxicity, low cost, and environmental protection. In order to explore the further fluorescence properties of the as-prepared NR nanodispersions, a detailed photoluminescent study with different NR concentrations ranging from 1 to 10 μg/mL was performed. As shown in Figure 8b, as the NR concentration increased, the fluorescence intensities of both nanodispersions prepared by RPB and ST have a rapid increase, followed by a decrease for a higher concentration. For the RPB sample, its fluorescence intensity reached a highest value of 1.86×10^6 at a NR concentration of 6 μg/mL, and then the reduction was only very slight. However, for the ST sample, its fluorescence intensity reached a highest value of 1.60×10^6 at a lower concentration of 4 μg/mL, and then displayed an obvious decrease. Such differences of NR concentration and fluorescence intensity prove the advantages of NR dispersions prepared by RPB. More importantly, it can be seen from the inset in Figure 8b that raw NR cannot fluoresce in aqueous solution. NR nanodispersions prepared by RPB have a higher fluorescence intensity than that of ST at the same concentration of 6 $g \cdot mL^{-1}$. This is because NR fluoresces only when it is well dissolved or dispersed in a solution, but cannot fluoresce in an aggregated state, owing to the occurrence of aggregation-caused quenching.[48] Since NR nanoparticles prepared by RPB have higher saturation solubility and better dispersity, this generates the stronger fluorescence intensity. Figure S9 shows the fluorescence quantum yields of NR nanodispersions with different NR concentrations prepared by RPB and ST. The result further indicates the aggregation-induced quenching effect of NR, and demonstrates that the performance of NR nanoparticles prepared by RPB is better than the ST counterpart.

Due to its properties of small size, high monodispersity and fluorescence in aqueous solution, the as-prepared aqueous NR nanodispersions were used for counterfeit labeling by adding it into ink. For this purpose, NR nanodispersion was added to a commercial ink (Picasso ps-906) to form a homogeneous mixture, and used to draw fluorescent patterns on paper. Figure 9 displays the photographs of patterns drawn using NR nanodispersion and NR fluorescent ink, and the corresponding fluorescence spectra of NR nanoparticles in the solid state. After the NR nanodispersion was drawn directly onto paper, the NR pattern adhered well to commercially available papers and was colorless under sunlight (Figure 9a), whereas it was red under UV light excitation at 254 nm (Figure 9b). After drawing with fluorescent ink containing NR nanodispersion (Figure 9c), the NR pattern shows red fluorescence under 254 nm UV lamp excitation (Figure 9d), and has a significant fluorescence emission broad peak at a wavelength range of 570–750 nm. While the paper shows negligible background fluorescence over the same wavelength range (Figure 9e). After continuous illumination under a UV lamp (254 nm) for 1 hr, the NR pattern still presented a clear fluorescence signal, indicating that the NR ink was photostable (Figure S10). These results suggest that NR nanodispersions are promising to be used in counterfeit labeling, solid-state fluorescent sensing and fluorescent composites.

NR aqueous nanodispersions can also be utilized for in vitro optical bioimaging of cells. The in vitro cytotoxicity of NR nanodispersions against CaCo-2 cells was investigated. The results of Figure S11 indicated that NR nanodispersions had a low cytotoxicity and good biocompatibility. Furthermore, in vitro cellular imaging was also investigated by confocal laser scanning microscope (CLSM). The red fluorescence of NR was clearly observed from the CaCo-2 cells, indicating that NR

nanoparticles were effectively taken up by cells (Figure S12b). Simultaneously, control cells (Figure S12a) showed no red fluorescence. The above results prove that NR nanodispersions have a great potential for use in fluorescence imaging.

4 | CONCLUSIONS

In summary, we have developed a novel high-gravity-assisted approach for controllable preparation of transparent aqueous nanodispersions of water-insoluble organic fluorescent dye NR with monodispersed and uniform nanoparticles. Due to the intensified micro-mixing during the antisolvent preparation process in the RPB, the prepared NR nanoparticles exhibited a much smaller average size of 35 nm, narrower size distribution, higher saturation solubility and stronger fluorescence compared with those of ST. Compared with raw NR, the resultant NR nanoparticles are well dispersed in an aqueous solution to emit stronger fluorescence owing to their reduced particle size and excellent dispersity. In addition, the nanodispersion was uniformly mixed with commercial ink for fluorescent pattern drawing, exhibiting bright red light under a 254 nm UV lamp. Therefore, it is envisioned that the developed route has possibilities to be expanded for other hydrophobic organic fluorescent dye in multifunctional applications.

ORCID

Dan Wang https://orcid.org/0000-0002-3515-4590
Jie-Xin Wang https://orcid.org/0000-0003-0459-1621

REFERENCES

1. Peng HS, Chiu DT. Soft fluorescent nanomaterials for biological and biomedical imaging. *Chem Soc Rev*. 2015;44:4699-4722.
2. Spyrogianni A, Tiefenboeck P, Starsich FHL, et al. Near-UV activated, photostable nanophosphors for in vitro dosimetry and dynamic bioimaging. *AIChE J*. 2018;64:2947-2957.
3. Chen CL, Yu Y, Li CG, et al. Facile synthesis of highly water-soluble lanthanide-doped t-$LaVO_4$ NPs for antifake ink and latent fingermark detection. *Small*. 2017;13:1702305.
4. Zhu SJ, Meng QN, Wang L, et al. Highly photoluminescent carbon dots for multicolor patterning, sensors, and bioimaging. *Angew Chem Int Ed*. 2013;52:3953-3957.
5. Li YC, Li XL, Chen DJ, et al. Design strategy of blue and yellow thermally activated delayed fluorescence emitters and their all-fluorescence white OLEDs with external quantum efficiency beyond 20%. *Adv Funct Mater*. 2016;26:6904-6912.
6. Reschgenger U, Grabolle M, Cavalierejaricot S, Nitschke R, Nann T. Quantum dots versus organic dyes as fluorescent labels. *Nat Methods*. 2008;5:763-775.
7. Fan JL, Wang SZ, Sun W, et al. Anticancer drug delivery systems based on inorganic nanocarriers with fluorescent tracers. *AIChE J*. 2018;64:835-859.
8. Qiu H, Gao L, Wang JX, Pan JM, Yan YS, Zhang XF. A precise and efficient detection of Beta-Cyfluthrin via fluorescent molecularly imprinted polymers with ally fluorescein as functional monomer in agricultural products. *Food Chem*. 2017;217:620-627.
9. Donmez M, Yilmaz MD, Kilbas B. Fluorescent detection of dipicolinic acid as a biomarker of bacterial spores using lanthanide-chelated gold nanoparticles. *J Hazard Mater*. 2016;324:593-598.
10. Bruchez M, Moronne M, Gin P, Weiss S, Alivisatos AP. Semiconductor nanocrystals as fluorescent biological labels. *Science*. 1998;281:2013-2016.
11. Rakovich A, Rackovich T. Semiconductor versus graphene quantum dots as fluorescent probes for cancer diagnosis and therapy applications. *J Mater Chem B*. 2018;6:2690-2712.
12. Chen GY, Qiu HL, Prasad PN, Chen X. Upconversion nanoparticles: design, nanochemistry, and applications in theranostics. *Chem Rev*. 2014;114:5161-5214.
13. Zhan QQ, Zhang X, Zhao YX, Liu J, He SL. Tens of thousands-fold upconversion luminescence enhancement induced by a single gold nanorod. *Laser Photon Rev*. 2015;9:479-487.
14. Wang D, Wang ZY, Zhan QQ, et al. Facile and scalable preparation of fluorescent carbon dots for multifunctional applications. *Engineering*. 2017;3:402-408.
15. Reineck P, Gibson BC. Near-infrared fluorescent nanomaterials for bioimaging and sensing. *Adv Opt Mater*. 2016;5:1600446.
16. Baker SN, Baker GA. Luminescent carbon nanodots: emergent nanolights. *Angew Chem Int Ed*. 2010;49:6726-6744.
17. Reisch A, Klymchenko AS. Fluorescent polymer nanoparticles based on dyes: seeking brighter tools for bioimaging. *Small*. 2016;12:1968-1992.
18. Wang D, Qian J, He SL, et al. Aggregation-enhanced fluorescence in PEGylated phospholipid nanomicelles for in vivo imaging. *Biomaterials*. 2011;32:5880-5888.
19. Yao H, Ashiba K. Highly fluorescent organic nanoparticles of thiacyanine dye: a synergetic effect of intermolecular H-aggregation and restricted intramolecular rotation. *RSC Adv*. 2011;1:834-838.
20. Pan J, Wan D, Bian Y, et al. Fluorescent hydroxyapatite-loaded biodegradable polymer nanoparticles with folate decoration for targeted imaging. *AIChE J*. 2013;59:4494-4501.
21. Corrias F, Schlich M, Sinico C, et al. Nile red nanosuspensions as investigative model to study the follicular targeting of drug nanocrystals. *Int J Pharm*. 2017;524:1-8.
22. Yao H, Yamashita M, Kimura K. Organic styryl dye nanoparticles: synthesis and unique spectroscopic properties. *Langmuir*. 2009;25:1131-1137.
23. Ke DM, Zhan CL, Xu SP, et al. Self-assembled hollow nanospheres strongly enhance photoluminescence. *J Am Chem Soc*. 2011;133:11022-11025.
24. Xu ZZ, Liao Q, Shi Q, Zhang HL, Yao JN, Fu HB. Low-threshold nanolasers based on slab-nanocrystals of H-aggregated organic semiconductors. *Adv Mater*. 2012;24:216-220.
25. Zhang XY, Zhang XQ, Yang B, et al. Fabrication of aggregation induced emission dye-based fluorescent organic nanoparticles via emulsion polymerization and their cell imaging applications. *Polym Chem*. 2013;5:399-404.
26. Soleilhac A, Girod M, Dugourd P, et al. Temperature response of rhodamine B-doped latex particles. From solution to single particles. *Langmuir*. 2016;32:4052-4058.
27. Li B, Kawakami T, Hiramatsu M. Enhancement of organic nanoparticle preparation by laser ablation in aqueous solution using surfactants. *Appl Surf Sci*. 2003;210:171-176.
28. Zhao YS, Peng AD, Fu HB, Yao JN. Nanowire waveguides and ultraviolet lasers based on small organic molecules. *Adv Mater*. 2008;20:1661-1665.
29. Atkinson EJO, Gilbert BD, Carlson ER. Detection of 4′,6-diamidino-2-phenylindole within silver-doped silica sol- and aerogels using surface-enhanced Raman spectroscopy. *J Non Cryst Solids*. 2014;405:16-20.
30. Jana A, Devi KSP, Maiti TK, Singh NDP. Perylene-3-ylmethanol: fluorescent organic nanoparticles as a single-component photoresponsive nanocarrier with real-time monitoring of anticancer drug release. *J Am Chem Soc*. 2012;134:7656-7659.

31. Stevens AL, Kaeser A, Schenning APHJ, Herz LM. Morphology-dependent energy transfer dynamics in fluorene-based amphiphile nanoparticles. *ACS Nano*. 2012;6:4777-4787.
32. Zhang ZB, Shen ZG, Wang JX, Zhao H, Chen JF, Yun J. Nanonization of megestrol acetate by liquid precipitation. *Ind Eng Chem Res*. 2009; 48:8493-8499.
33. Chen JF, Wang YH, Guo F, Wang XM, Zheng H. Synthesis of nanoparticles with novel technology: high-gravity reactive precipitation. *Ind Eng Chem Res*. 2000;39:948-954.
34. Zheng XH, Chu GW, Kong DJ, et al. Mass transfer intensification in a rotating packed bed with surface-modified nickel foam packing. *Chem Eng J*. 2016;285:236-242.
35. Rao DP, Bhowal A, Goswami PS. Process intensification in rotating packed beds (HIGEE): an appraisal. *Ind Eng Chem Res*. 2004;43:1150-1162.
36. Liu YP, Wu K, Wang JX, Le Y, Zhang LL. Continuous production of antioxidant liposome for synergistic cancer treatment using high-gravity rotating packed bed. *Chem Eng J*. 2018;334:1766-1774.
37. Sun Q, Chen B, Wu X, et al. Preparation of transparent suspension of lamellar magnesium hydroxide nanocrystals using a high-gravity reactive precipitation combined with surface modification. *Ind Eng Chem Res*. 2015;54:666-671.
38. Yu L, Li CX, Le Y, Chen JF. Stabilized amorphous glibenclamide nanoparticles by high-gravity technique. *Mater Chem Phys*. 2011;130: 361-366.
39. Chen JF, Shao L, Guo F, Wang XM. Synthesis of nanofibers of aluminum hydroxide in novel rotating packed bed reactor. *Chem Eng Sci*. 2003;58:569-575.
40. Hu K, Mcclements DJ. Fabrication of surfactant-stabilized zein nanoparticles: a pH modulated antisolvent precipitation method. *Food Res Int*. 2014;64:329-335.
41. Matteucci ME, Hotze MA, Johnston KP, Williams RO. Drug nanoparticles by antisolvent precipitation: mixing energy versus surfactant stabilization. *Langmuir*. 2006;22:8951-8959.
42. Galisteo-González F, Molina-Bolívar JA. Systematic study on the preparation of BSA nanoparticles. *Colloids Surf B*. 2014;123:286-292.
43. Horn D, Rieger J. Organic nanoparticles in the aqueous phase-theory, experiment, and use. *Angew Chem Int Ed*. 2001;40:4330-4361.
44. Paria S, Khilar KC. A review on experimental studies of surfactant adsorption at the hydrophilic solid–water interface. *Adv Colloid Interface Sci*. 2004;110:75-95.
45. Kim MJ, Huh YD. Synthesis and optical properties of $CaMoO_4$:Eu^{3+}, Na^+ nanophosphors and a transparent $CaMoO_4$: Eu^{3+}, Na^+ suspension. *Opt Mater*. 2012;35:263-267.
46. Müller H, Peters K. Nanosuspensions for the formulation of poorly soluble drugs: I preparation by a size-reduction technique. *Int J Pharm*. 1998;160:229-237.
47. Liu MT, Wang TL, Ma HW, Fu Y, Hu KR, Guan C. Layer-by-layer assembly of luminescent multilayer thin films by MMT, anionic chromophores and magnetic CoAl-LDHs nanosheets. *Mater Lett*. 2015;153:40-43.
48. Mei J, Leung NLC, Kwok RTK, Lam JWY, Tang BZ. Aggregation-induced emission: together we Shine, united we soar! *Chem Rev*. 2015;115:11718-11940.

SUPPORTING INFORMATION

Additional supporting information may be found online in the Supporting Information section at the end of this article.

How to cite this article: Yin X, Sun Q, Wang D, et al. High-gravity-assisted synthesis of aqueous nanodispersions of organic fluorescent dyes for counterfeit labeling. *AIChE J*. 2019;65:e16714. https://doi.org/10.1002/aic.16714